# The influence of water of hydrolysis on microstructural development in sol-gel derived $LiNbO_3$ thin films

Vikram Joshi
*Department of Chemical Engineering and Materials Science, University of Minnesota, Minneapolis, Minnesota 55455*

Martha L. Mecartney
*Materials Science and Engineering Program, Department of Mechanical and Aerospace Engineering, University of California, Irvine, California 92717*

(Received 31 March 1993; accepted 15 June 1993)

The effect of water of hydrolysis on nucleation, crystallization, and microstructural development of sol-gel derived single phase $LiNbO_3$ thin films has been studied using transmission electron microscopy (TEM), atomic force microscopy (AFM), x-ray diffraction (XRD), and differential scanning calorimetry (DSC). A precursor solution of double ethoxides of lithium and niobium in ethanol was used for the preparation of sol. DSC results indicated that adding water to the solution for hydrolysis of the double ethoxides lowered the crystallization temperature from 500 °C (no water) to 390 °C (2 moles water per mole ethoxide). The amount of water had no effect on the short-range order in amorphous $LiNbO_3$ gels but rendered significant microstructural variations for the crystallized films. AFM studies indicated that surface roughness of dip-coated films increased with increasing water of hydrolysis. Films on glass, heat-treated for 1 h at 400 °C, were polycrystalline and randomly oriented. Those made with a low water-to-ethoxide ratio had smaller grains and smaller pores than films prepared from sols with higher water-to-ethoxide ratios. Annealing films with a low water concentration for longer times or at higher temperatures resulted in grain growth. Higher temperatures (600 °C) resulted in grain faceting along close-packed planes. Films deposited on c-cut sapphire made with a 1 : 1 ethoxide-to-water ratio and heat-treated at 400 °C were epitactic with the c-axis perpendicular to the film-substrate interface. Films with higher concentrations of water of hydrolysis on sapphire had a preferred orientation but were polycrystalline. It is postulated that a high amount of water increases the concentration of amorphous $LiNbO_3$ building blocks in the sol through hydrolysis, which subsequently promotes crystallization during heat treatment.

## I. INTRODUCTION

Lithium niobate is an important ferroelectric material due to its unique properties, such as a very high spontaneous polarization, a very high Curie temperature (1210 °C), and a large negative birefringence.[1–3] Thin films of $LiNbO_3$ are of current research interest because of the demand for active integrated optical devices.[4–6] Sol-gel processing promises to be a viable process technique for growing $LiNbO_3$ films on various substrates as it facilitates both lowering the temperature of crystallization and obtaining the correct stoichiometry.[7–9] Processing parameters such as solution chemistry, deposition technique, firing conditions, and substrate are known to influence the development of film crystallinity, porosity, grain size, and growth morphology during sol-gel processing.[10–12] It has also been shown that the structure of sol-gel derived $LiNbO_3$ thin films sensitively depends on the prior processing.[13] In order to produce optimal film microstructures for practical applications of ferroelectric thin films in electrical and optical systems, the connection between processing and the resultant microstructure is essential. The objective of this work, therefore, was to investigate the effect of specific processing parameters on the microstructural development and crystallization of $LiNbO_3$ thin films made from double metal alkoxide solutions.

In particular, the water of hydrolysis was considered critical to investigate with respect to its effect on the nucleation and crystallization process and the consequent microstructural development of the $LiNbO_3$ phase from the amorphous gel. Water is deliberately added to promote hydrolysis and condensation, but water is present also in the atmosphere and is a by-product of hydrolysis and condensation. Much of the research on water concentration effects on sol-gel derived ferroelectric thin films has focused on x-ray diffraction (XRD) studies of crystallization and phase development with little attention to microstructural details.[9,12] Hirano and

 

Kato[14] have shown that heat treatment of sol-gel derived $LiNbO_3$ thin films in an atmosphere of water vapor and $O_2$ helps in lowering the crystallization temperature. XRD studies by Nashimoto and Cima[9] reported increased orientation of $LiNbO_3$ films on sapphire with reduced water levels in the sol, unhydrolyzed sol yielding epitaxial films. These studies indicate a significant role for water in crystallization, but it is not yet understood how the degree of hydrolysis controls microstructural development.

A second parameter chosen to investigate was the relationship between the choice of substrate and the crystallization behavior. Amorphous silicate glass substrates were chosen in order to study nucleation and grain morphology in polycrystalline $LiNbO_3$ films. Thin films were also deposited on c-cut sapphire substrates for epitaxial crystallization. These latter substrates should promote optimal orientation for certain device applications. Bulk gels, unconstrained by substrates, were also studied to compare their nucleation and crystallization behavior with thin films.

## II. EXPERIMENTAL

Based on the method outlined by Hirano and Kato,[14] a 0.5 M stock solution of double metal ethoxide was prepared by refluxing lithium and niobium ethoxide in ethanol for 24 h. Small portions of the stock solution were partially hydrolyzed by using an ethanol-water mixture to induce gelation. Three different water concentrations were used for hydrolysis: 1, 2, and 3 moles of water for each mole of ethoxide. The obtained gels were air dried at room temperature and were characterized by transmission electron microscopy (TEM) and differential scanning calorimetry (DSC). DSC was performed in air for partially hydrolyzed gels and in both air and nitrogen for unhydrolyzed powders at heating rates of 10 °C/min.

Spinnable solutions of 0.25 molarity were prepared by dilution of the stock solution with an ethanol-water mixture. Sols with no water, 1:1, and 1:2 ethoxide-to-water ratios were prepared. Sols having an ethoxide-to-water ratio of 1:3 showed such a rapid increase in viscosity and quick gelation so that no films could be spun. Microscope glass slides and c-cut sapphire (Insaco Inc., Quakertown, PA) were cleaned ultrasonically in acetone, 20% HCl solution, and de-ionized water in that order. The substrates were heat-treated up to 350 °C for 15 min and then cooled down to room temperature right before the coating was started in order to decompose any residual on the surface of the substrate.

Glass substrates were dip coated in the precursor solution and were withdrawn at a speed of 5 cm/min. Sapphire substrates were spin coated at 2000 rpm. Each coating layer was dried at 300 °C on a hot plate for 1 min and produced a film thickness of about 60 nm for dip coating and 40 nm for spin coating. The coating and heating steps were repeated as many times as necessary to achieve a desired thickness, usually approximately 150 nm. As-deposited $LiNbO_3$ thin films were then heated to temperatures from 400 °C to 600 °C at a ramp rate of 10 °C/min in an air ambient, maintained at the annealing temperature for times from 1 to 4 h, and then furnace cooled.

Microstructural characterization of the films was primarily accomplished by TEM. Specimens for TEM analysis were prepared using standard specimen preparation techniques for cutting, polishing, dimpling, and ion milling. Cryo-TEM samples were prepared according to the technique described by Bailey *et al.*[15] TEM work was carried out on JEOL 100CX, Philips CM30, and Philips CM20 transmission electron microscopes. A double tilt cold stage cooled with liquid nitrogen was used in order to reduce electron beam heating effects. The use of plan-view geometries enabled observation of the film microstructure while obtaining electron diffraction information about the in-plane orientation of the film.

## III. RESULTS

### A. Microstructure of wet and dried films

Figure 1 shows the cryogenic transmission electron micrograph and corresponding selected area diffraction (SAD) pattern of the frozen sol with an ethoxide-to-water ratio of 1:2 at 75% of the gelation time. A rather featureless microstructure and a diffuse halo in

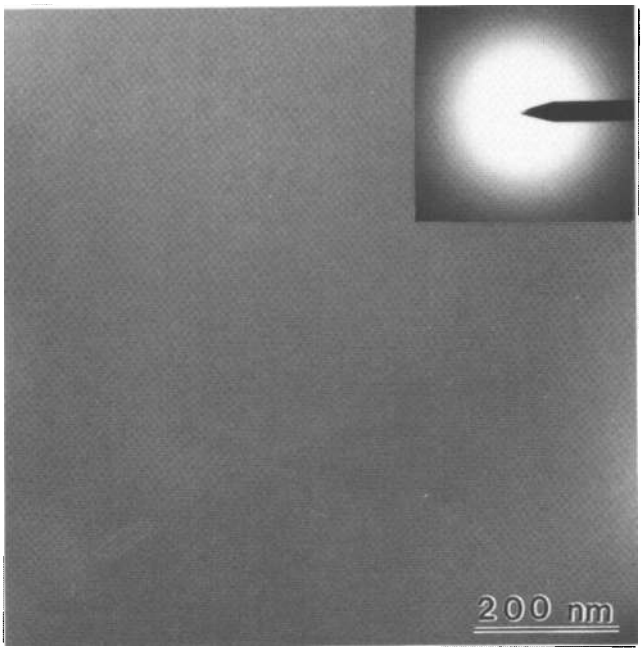


FIG. 1. Cryogenic transmission electron micrograph illustrating the microstructure of a 1:2 $LiNb(OC_2H_5)_6/H_2O$ sol at 75% of gelation time. SAD pattern represents the amorphous nature of the sol.

the SAD pattern are observed. No phase separation or precipitate formation in this partially hydrolyzed sol is observed.

TEM micrographs of films of lithium niobium ethoxide sols deposited on holey carbon TEM grids are shown in Fig. 2. These micrographs give the first indication of variations between different ethoxide-to-water ratios. An increase in the amount of water of hydrolysis results in an increased pore size for these thin film gels. The film deposited from unhydrolyzed sol is of uniform thickness and very dense. Pores on the order of 5 nm or less are visible in the 1:1 film, whereas the 1:2 film is even coarser with pore size varying between 2 and 10 nm. Diffuse halos in the SAD patterns were analyzed for short-range order in these amorphous films. The interatomic distances corresponding to the maximum intensity of the first and second strongest halos are 3.7 Å and 2.0 Å, respectively, for all samples, even with differing amounts of water. These two halos were present in all three types of samples, although difficult to see in Fig. 2 due to different exposure times.

### B. Thermal analysis

The crystallization kinetics of the amorphous gels was studied by DSC. Figure 3 shows DSC traces from 200 to 600 °C for gels formed under different hydrolysis conditions. Below this temperature range, all compositions had an endothermic peak at about 100 °C, associated with the removal of residual solvent and water. Exothermic transformations are observed in the 200 to 600 °C region. The exothermic peak around 325 °C is associated with a weight loss, as observed by TGA. This weight loss, which could be interpreted as corresponding to the decomposition of bound organic species, precedes an exothermic transformation at temperatures near 400 °C which represents crystallization of amorphous $LiNbO_3$ (as confirmed by the XRD results). The exothermic peak temperatures are at 390 and 410 °C for the 1:2 and 1:1 gels, respectively. Unhydrolyzed powders crystallized at 500 °C when heated in a nitrogen atmosphere, but in air these powders showed two exotherms, at 400 °C and 500 °C. The two exotherms were most likely due to the fact that the highly reactive powder surfaces were probably partially

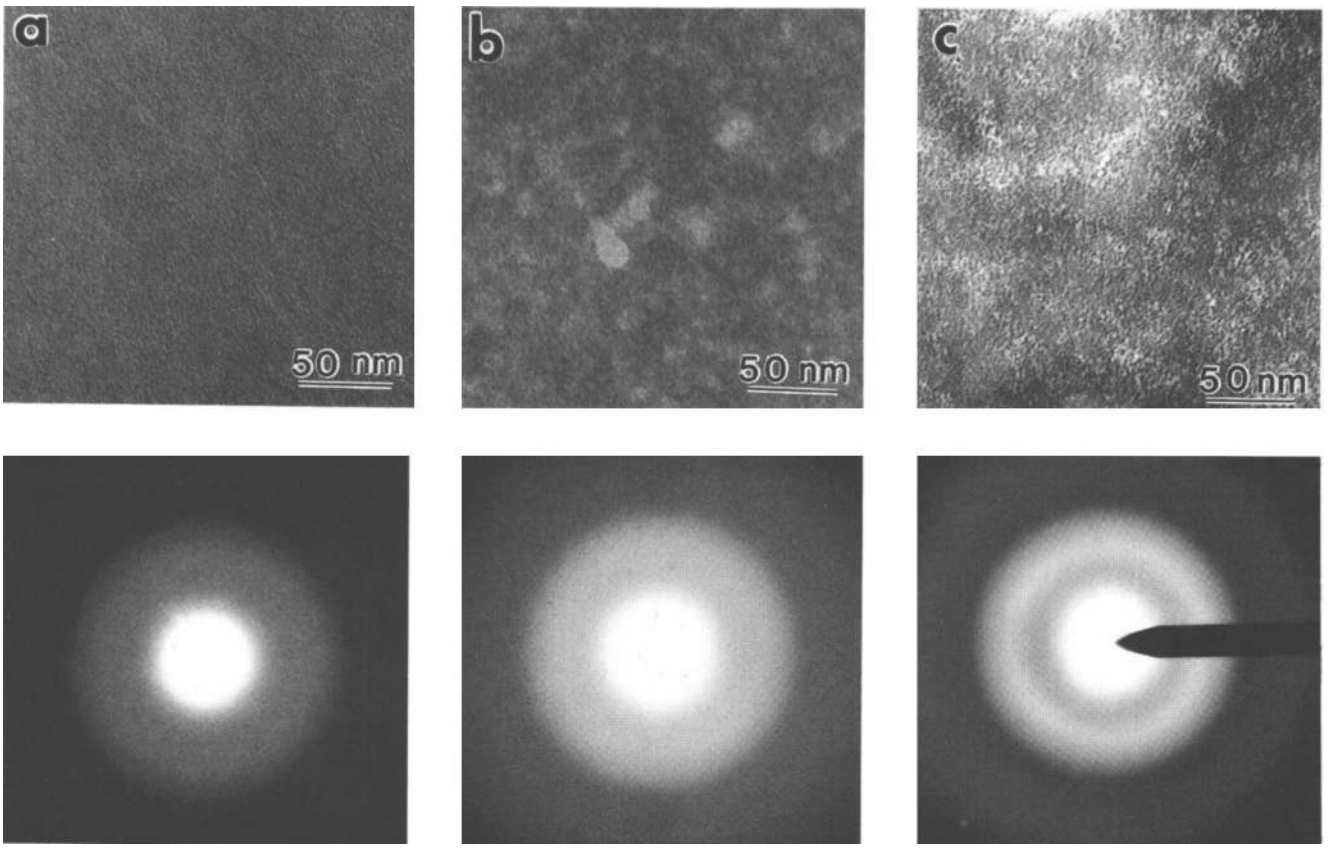


FIG. 2. Amorphous $LiNbO_3$ films with ethoxide/water ratios of (a) 1:0, (b) 1:1, and (c) 1:2. These images show nanometer scale porosity, which increases with increasing amounts of water in the sol. The corresponding SAD patterns show two diffuse rings.

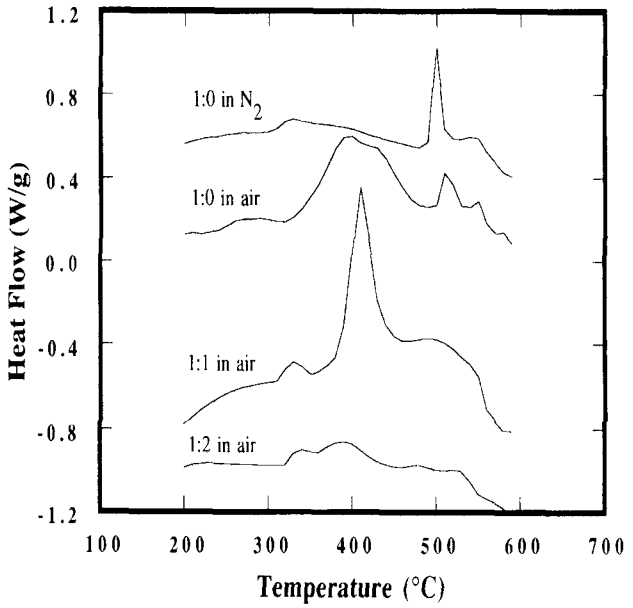


FIG. 3. Water of hydrolysis dependence of DSC curves for various $LiNbO_3$ gels.

hydrolyzed when heated in air, and so the two peaks would correspond to the crystallization of hydrolyzed and unhydrolyzed regions.

### C. Nucleation and crystallization in $LiNbO_3$ powders and gels

Phase formation and microstructural changes during the amorphous-to-crystalline transformation in 1 : 2 dried gel were observed in the transmission electron microscope. When a sample was heated to 200 °C very fine crystallites of $LiNbO_3$ of a size less than 20 nm nucleated in an amorphous matrix within 30 min [Fig. 4(a)]. The electron diffraction pattern of this area shows the appearance of distinct spots along with the presence of diffuse rings, indicating the onset of crystallization. The powders were further heated at a rate of 10 °C/min and were held at 400 °C for 30 min. At 450 °C, in certain samples spherical particles were formed [Fig. 4(b)]. These crystalline particles range in size from approximately 50–200 nm. At 600 °C, large crystallites on the order of 1 $\mu$m are observed [Fig. 4(c)]. The SAD pattern from one such particle is essentially that of a single crystal. The side facet faces are the first order prism planes, $\{10\bar{1}0\}$, and the top and bottom faces are basal planes (0001) (normal to the zone axis [0001]).

### D. Thin films on amorphous substrates

Atomic force microscopy (AFM) is a very useful technique for monitoring the surface topology of nonconducting surfaces.[16] AFM of $LiNbO_3$ thin films on glass was used to determine the effects of the amount of water of hydrolysis on surface roughness of films on glass (heat-treated at 400 °C). One can see in Fig. 5 that the dip-coated $LiNbO_3$ thin films after heat treatment at 400 °C for 1 h show increased surface roughness (on the order of 10 nm) as the ethoxide-to-water ratio changed from 1 : 1 to 1 : 2. Films deposited from unhydrolyzed (1 : 0) and 1 : 1 sols were extremely smooth (on the order of 2 nm).

Crystallization as a function of water of hydrolysis in 1200 Å thick $LiNbO_3$/glass films was studied by TEM analysis. Figure 6 shows TEM micrographs of $LiNbO_3$ films on glass fired at 400 °C for 1 h. The film deposited on glass using an unhydrolyzed sol was amorphous at 400 °C [Fig. 6(a)], but the films made with partially hydrolyzed sols crystallized at 400 °C [Figs. 6(b) and 6(c)]. The 1 : 1 film appears relatively dense with a grain size in the range of 20–30 nm. The selected area diffraction (SAD) pattern indicates the polycrystalline nature of the film. The rings in the SAD pattern index to the $d$ spacings of the $LiNbO_3$ crystal structure. A very different microstructure was observed for the 1 : 2 film. Distinctive microstructural features of this film are large pores and a large grain size on the order of 150 nm. The pore and the grain size are of similar size and the pores

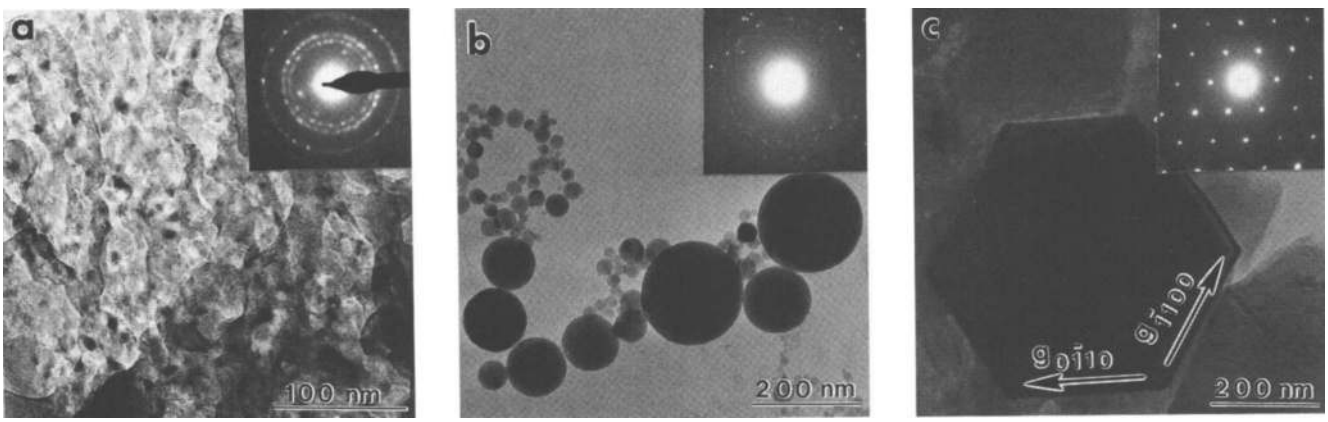


FIG. 4. Transmission electron micrographs and corresponding SAD patterns of $LiNbO_3$ bulk gels (a) 200 °C, (b) 450 °C, and (c) 600 °C.

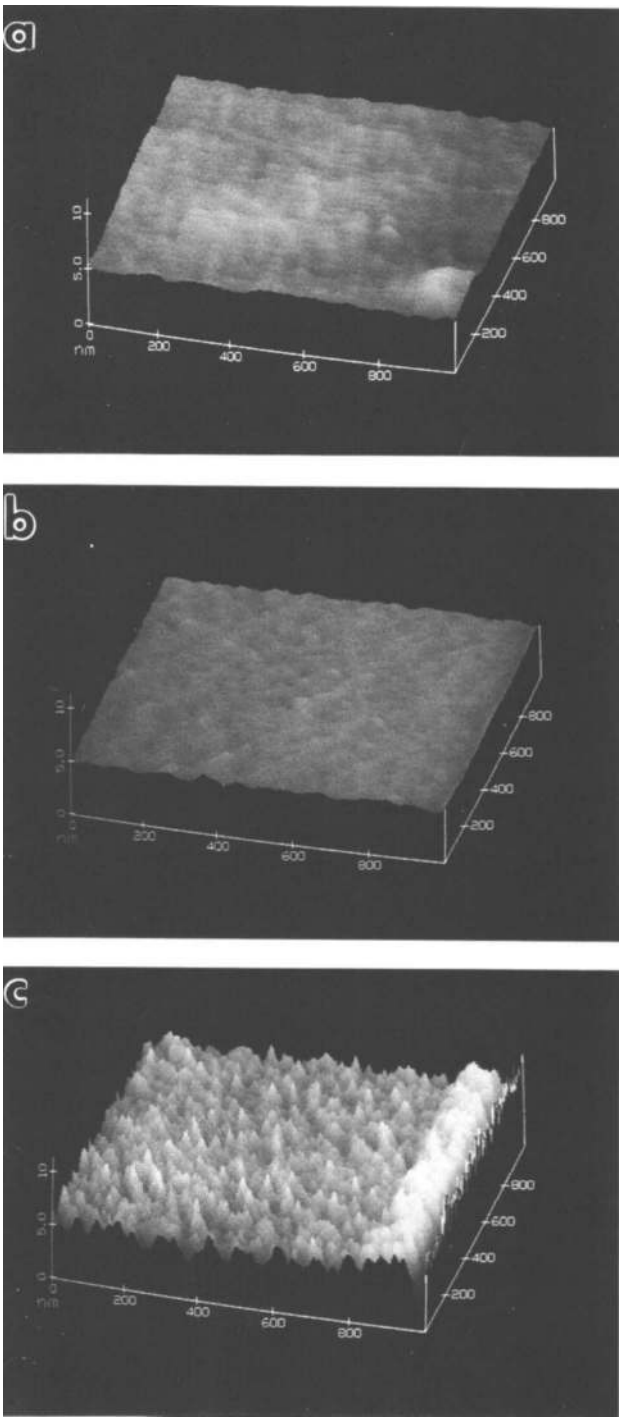


FIG. 5. Atomic force micrographs of $LiNbO_3$ films on glass substrates with ethoxide/water ratios of (a) 1:0, (b) 1:1, and (c) 1:2. All the films were annealed at 400 °C for 1 h.

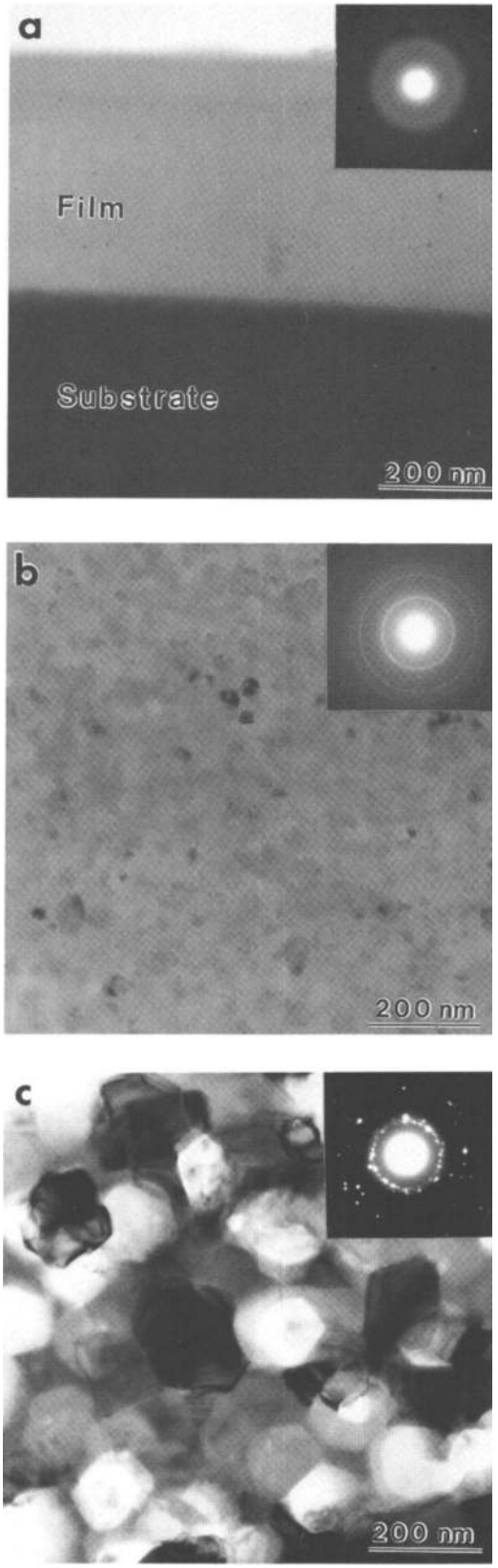


FIG. 6. Variation in microstructure with ethoxide/water ratio for $LiNbO_3$ films on glass substrates (a) 1:0, (b) 1:1, and (c) 1:2. All the films were annealed at 400 °C for 1 h.

appear as holes in the 120 nm thick film [Fig. 6(c)]. Twins or stacking faults are observed in some grains.

The influence of annealing temperature in 1:1 film microstructure is shown in Fig. 7(a). With heat treatments, the average crystallite size in the film increased

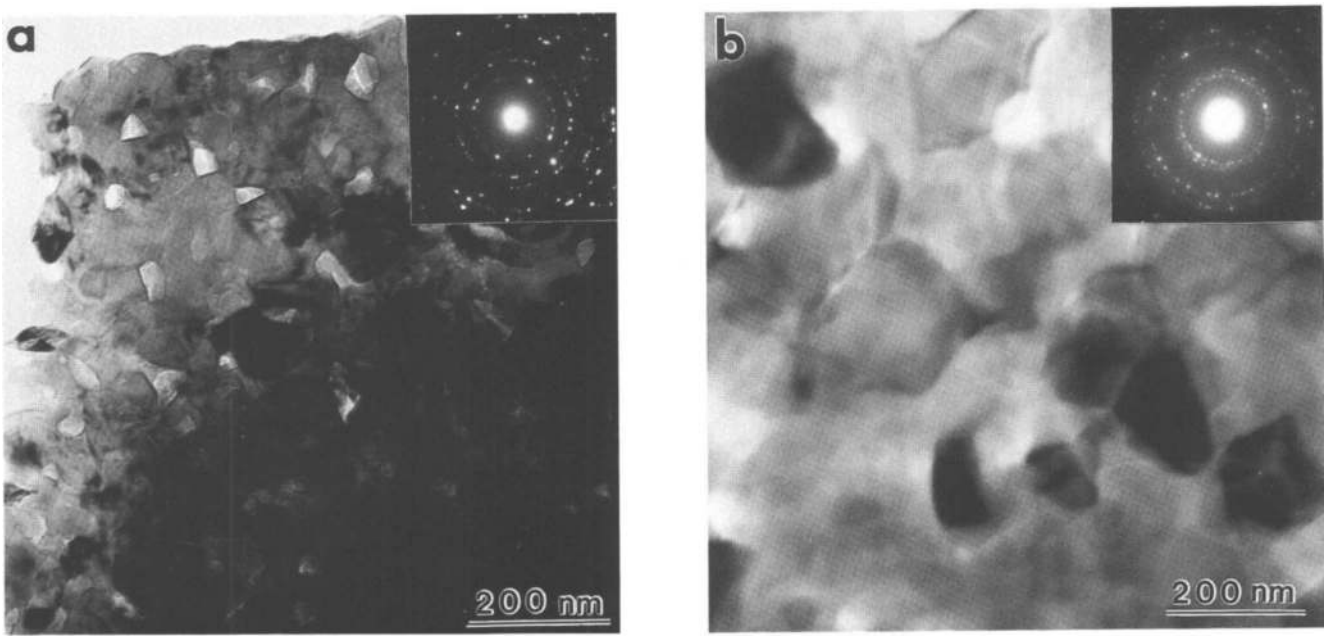


FIG. 7. Crystallized 1 : 1 $LiNbO_3$ thin films on glass: (a) effect of higher temperature, 600 °C, for 1 h and (b) effect of longer soaking time, 400 °C, for 4 h.

from 30 nm at 400 °C to 125 nm at 600 °C for 1 h. More diffraction rings are observed in the SAD pattern of this film compared to the films heat-treated at 400 °C for 1 h. The excess rings indexed to the Li deficient phase $LiNb_3O_8$.

Figure 7(b) shows the microstructure of 1 : 1 $LiNbO_3$ film on a glass substrate annealed at 400 °C for 4 h. Compared to Fig. 7(a) (600 °C, 1 h), these longer heat-treatment times result in grain growth but no development of any second phase. The SAD pattern of this film confirms the presence of single phase $LiNbO_3$. After 4 h of soaking time, the average grain size in the 1 : 1 film was on the order of 150 nm, similar to the grain size observed in the 1 : 2 film, annealed at 400 °C for 1 h. However, the 1 : 1 film at 400 °C for 4 h remained relatively dense and free of large pores, unlike the microstructure of the 1 : 2 film at 400 °C for 1 h.

### E. Thin films on (0001) sapphire substrates

$LiNbO_3$ thin films on (0001) sapphire were also examined by TEM and XRD. Figures 8 and 9 show regions of a film spun-coated using a sol with $LiNb(OC_2H_5)_6 : H_2O$ ratio of 1 : 1 and annealed at 400 °C for 1 h. The underlying substrate was completely removed during ion milling. Figure 8 shows a typical bright-field and dark-field image of a $LiNbO_3$ thin film on (0001)-oriented sapphire. The prominent features of this film are its single crystal nature and absence of porosity. The sharp diffraction spots of the [0001] zone axis in Fig. 8(a) indicate growth well oriented with respect to the substrate. However, Fig. 9 shows another area of this film, where twinning along the $[10\bar{1}0]$ direction is observed. Thickness fringes and dislocations are also noticeable in the images shown in Figs. 8 and 9.

Figure 10(a) is a high magnification image of a region where the film was still attached to the substrate. Moiré fringes are observed in this micrograph. Figure 10(b) shows the corresponding SAD pattern taken with the electron beam parallel to the sapphire [0001] zone axis. This SAD pattern demonstrated that the $LiNbO_3$ thin film was epitaxially grown onto the sapphire substrate with the following orientation relationship:

$$(0001)LiNbO_3 // (0001) \text{ sapphire and}$$
$$[11\bar{2}0]LiNbO_3 // [11\bar{2}0] \text{ sapphire}$$

The lattice mismatch for this relationship is 7.5% ($a = 0.5149$ nm, $c = 1.3862$ nm for $LiNbO_3$ and $a = 0.4758$ nm, $c = 1.2991$ nm for sapphire).

An increase in the water of hydrolysis in the sol to 2 moles of water for each mole of ethoxide results in a very different microstructure of $LiNbO_3$ film on c-cut sapphire. Figure 11 shows the TEM micrograph of such a film annealed at 400 °C for 1 h, with the same ramping rate. This film is polycrystalline with a grain size of 0.5 $\mu$m and micropores are entrapped within the grains. Similar micropores are also observed at the grain boundaries. X-ray data of the 1 : 2 film on sapphire showed a strong (0006) reflection of $LiNbO_3$ (Fig. 12), indicating a preferred growth direction. However, there is no in-plane alignment of the grains, and the rotation

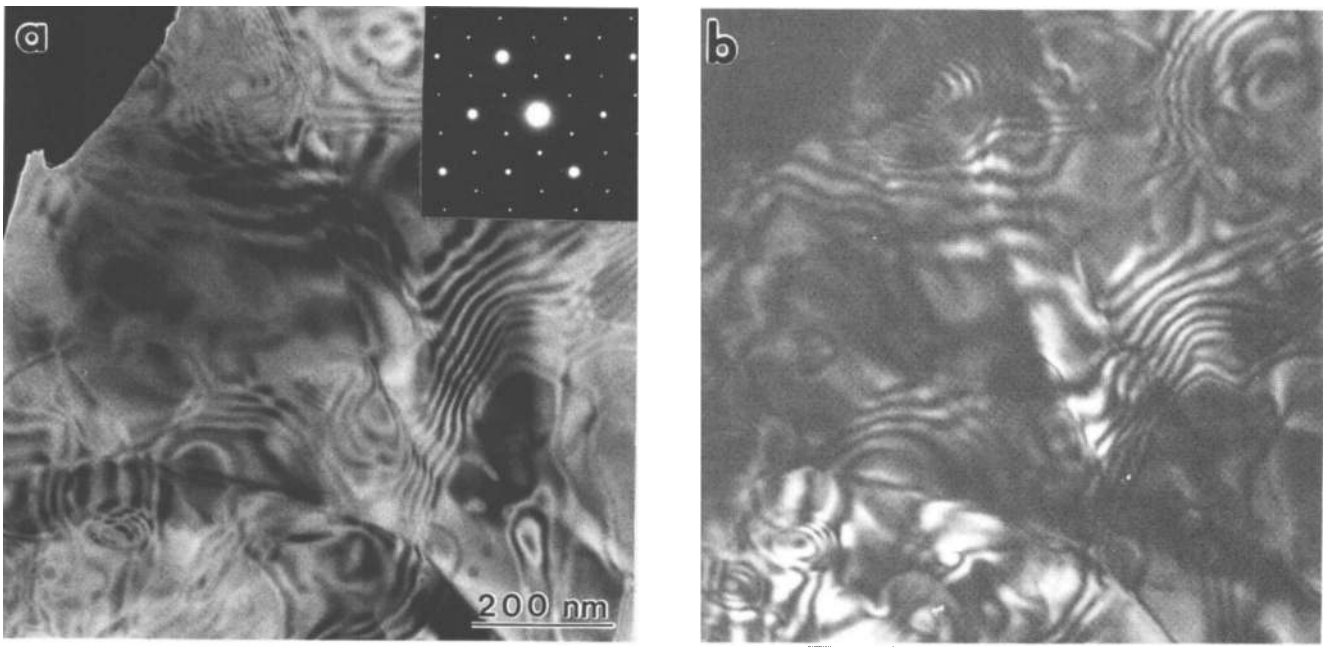


FIG. 8. (a) Bright-field and (b) dark-field images of single crystal 1 : 1 $LiNbO_3$ thin film on (0001) sapphire substrate, annealed at 400 °C for 1 h.

of the in-plane axes for the $LiNbO_3$ grains is evident in the SAD pattern of Fig. 11.

## IV. DISCUSSION

One of the most important results obtained in this study is the fact that water of hydrolysis influences many features including (a) temperature of crystallization, (b) latent heat of crystallization, (c) epitaxy, (d) grain size, and (e) the amount of porosity and pore size in sol-gel derived $LiNbO_3$ thin films. In some ways this result may seem surprising because the chemical short-range order in the amorphous films derived from the electron diffraction information was not affected by the amount of water of hydrolysis. Both unhydrolyzed and partially hydrolyzed dried films manifested similar maxima in the short-range order. The short-range order did not change even after the unhydrolyzed film on glass was treated at 400 °C for 1 h. However, a similar heat treatment rendered the partially hydrolyzed films on glass and sapphire substrates crystalline.

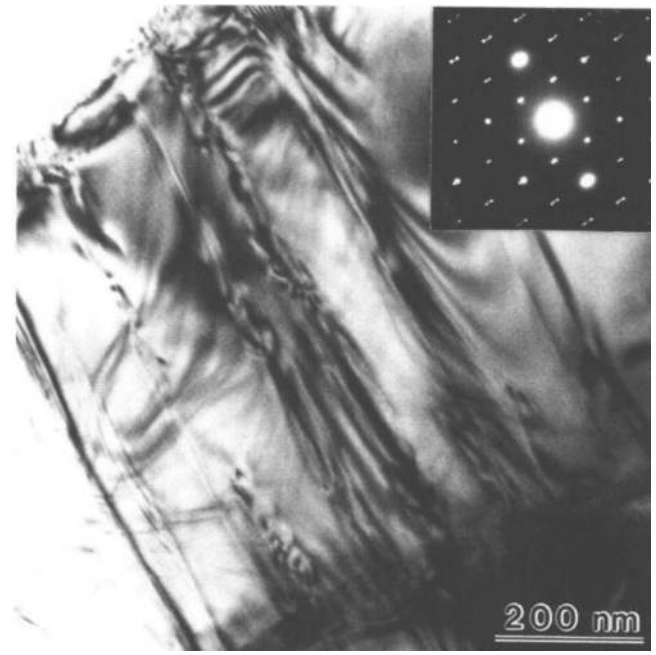


FIG. 9. Twinning in $[10\bar{1}0]$ direction as evidenced in the SAD pattern of 1 : 1 $LiNbO_3$ thin film on sapphire. Zone axis = [0001].

Short-range order in an amorphous phase is usually very similar to that of the crystal which will grow from the amorphous phase.[17] Prominent atomic pairs in the lithium niobium double ethoxide, $LiNb(OC_2H_5)_6$, can be related to the crystal structure of $LiNbO_3$. In this regard it is interesting to consider the results of XRD studies of $LiNb(OC_2H_5)_6$ and FTIR investigations of amorphous $LiNbO_3$ gels by Eichorst and Payne.[18] Their results showed that structure of $LiNb(OC_2H_5)_6$ is composed of alternating $Nb(OC_2H_5)_6$ octahedra linked by severely distorted tetrahedrally coordinated Li atoms. These structural features were maintained during gelation. NMR investigations have shown that it is the Li environment that shows a continuous change with increasing water content until the amount of water reaches the stoichiometric quantity needed for complete hydrolysis (3 moles per mole of ethoxide).[19] Although NMR results are not reported for the Nb environment with variations in the amount of water, our results suggest that

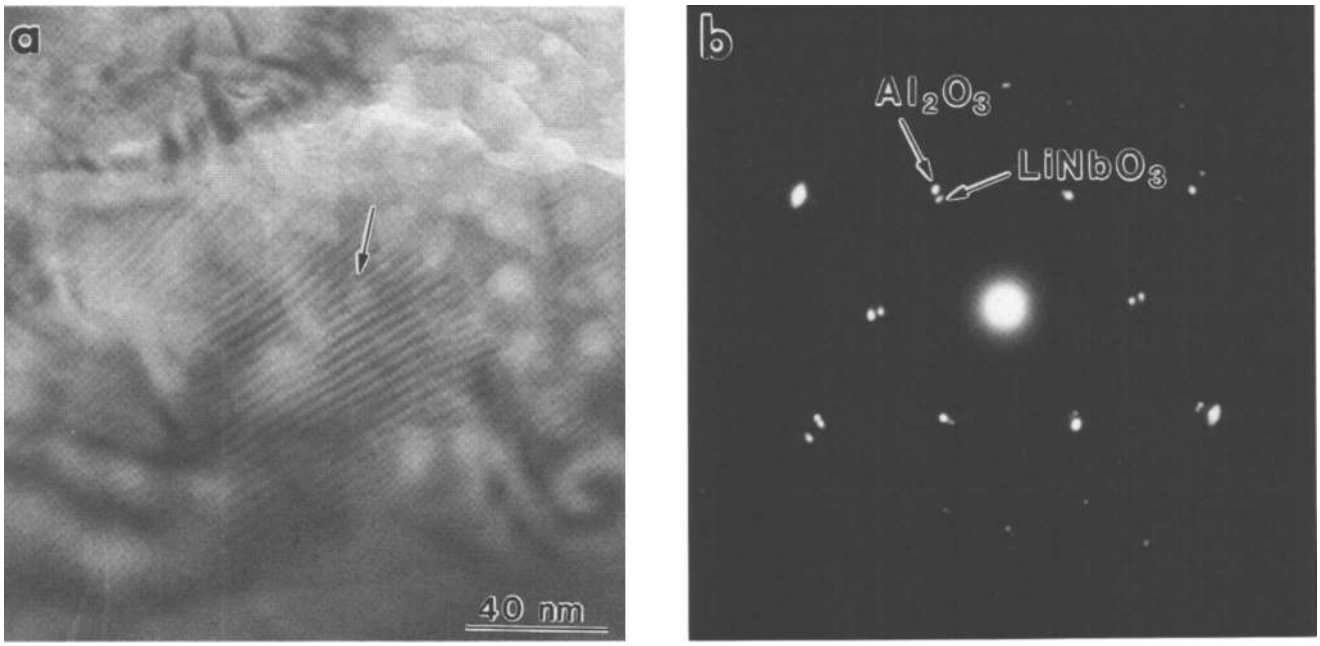


FIG. 10. (a) Moiré fringes revealing the misfit between (0001) oriented 1 : 1 $LiNbO_3$ film on (0001) sapphire. The arrow indicates a terminating fringe. (b) SAD pattern with electron beam parallel to sapphire [0001] zone axis.

the Nb octahedra are stable even with changing water concentration in the gel.

The structure of crystalline $LiNbO_3$ at temperatures below the ferroelectric Curie temperature (approximately 1210 °C) consists of planar sheets of oxygen atoms in a distorted hexagonal close-packed configuration. The octahedral interstices formed in this structure are one-third filled by lithium atoms, one-third filled by niobium atoms, and one-third vacant.[20] Since the Li atom goes through a change in its coordination state from tetrahedral in the double ethoxide to octahedral in crystalline lithium niobate while Nb remains octahedrally coordinated, it is the Li environment that experiences most

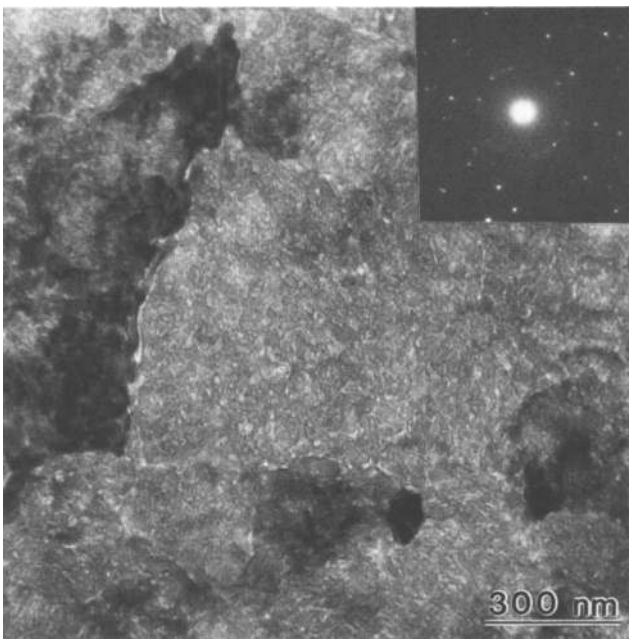


FIG. 11. TEM image of a 1 : 2 $LiNbO_3$ thin film on (0001) sapphire. Intergranular and intragranular porosity can be seen in the micrograph. Note the polycrystalline nature of this film in contrast to the film in Fig. 7.

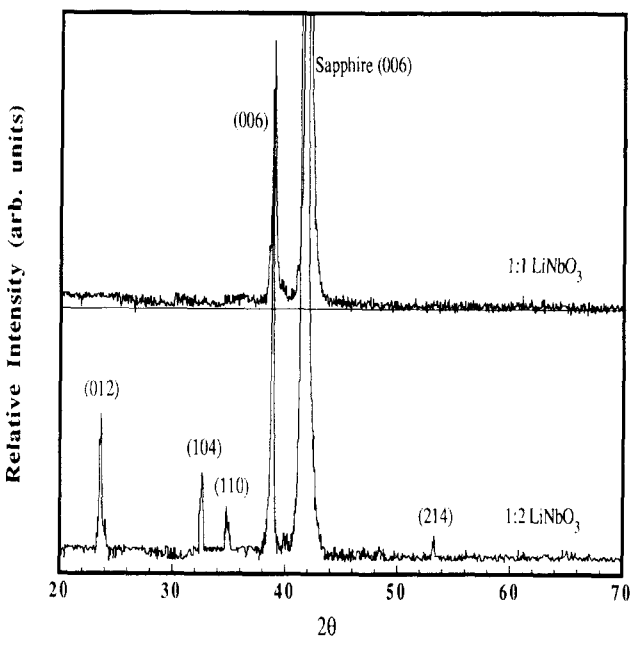


FIG. 12. XRD patterns of $LiNbO_3$ films on (0001) sapphire showing the effect of water of hydrolysis.

of the structural changes during the amorphous-to-crystalline transformation. If we consider the SAD patterns of amorphous films shown in Fig. 2, the interatomic distance $d_1 \approx 3.7$ Å corresponds to the theoretical values of the interatomic distances between Nb–Nb and Li–Li pairs in crystalline $LiNbO_3$, 3.765 Å. The interatomic distance $d_2 \approx 2.0$ Å may correspond to the two characteristic Nb–O spacings, 1.889 Å and 2.212 Å.[21] The average Nb–O (bridging) bond length in $LiNb(OC_2H_5)_6$, as reported by Eichorst *et al.* using XRD, is 1.98 Å.[22] It is apparent that the distances between these atomic pairs in the amorphous phase change only slightly during crystallization. This indicates that an important criterion for the low temperature crystallization of any phase through sol-gel processing may be the selection of a precursor species which not only has the right stoichiometry but also has a chemical short-range order that does not change significantly upon crystallization.

Having described the negligible effect that the water concentration has on the chemical short-range order of thin amorphous films of $LiNbO_3$ and the similarity in the local atomic arrangement of $LiNb(OC_2H_5)_6$ to that of crystalline $LiNbO_3$, we are left with the problem of explaining the dramatic microstructural variations due to changing the amount of water of hydrolysis for crystallized thin $LiNbO_3$ films on glass and sapphire. TEM results demonstrate that the amount of water present in the sol markedly influences the grain size and density in crystalline $LiNbO_3$ films on glass. The relative rates of hydrolysis and condensation are affected by the amount of water present. These in turn affect the rate of molecular rearrangement that (a) transform the double ethoxide to amorphous lithium niobate and (b) condense the molecules into an interconnected network. These two phenomena, which can be dealt with separately even though they may occur simultaneously, seem to be responsible for the final differences in grain size and porosity, respectively. Three effects of the degree of hydrolysis can be delineated for the purpose of discussion.

(1) The first stage of crystallization is associated with the hydrolysis of the double ethoxide resulting in the formation of amorphous $LiNbO_3$ which acts as a building block for crystalline $LiNbO_3$. The concentration of these building blocks in the sol is proportional to the degree of hydrolysis according to the equation,

$$LiNb(OC_2H_5)_6 + (3 - x/2)H_2O \rightarrow LiNbO_{3-x/2}(OC_2H_5)_x + xC_2H_5OH$$

The possible species produced by this reaction are $LiNbO_{1/2}(OC_2H_5)_5$, $LiNbO(OC_2H_5)_4$, $LiNbO_{3/2}(OC_2H_5)_3$, $LiNbO_2(OC_2H_5)_2$, $LiNbO_{5/2}(OC_2H_5)$, and $LiNbO_3$, depending on the amount of water added. In reality, the product of the above reaction is a mixture of these species, though some of them may not exist due to their thermodynamic instability. $LiNbO_2(OC_2H_5)_2$ and amorphous $LiNbO_3$ are known to be stable compounds.[18] Higher water ratios result in a higher concentration of the amorphous $LiNbO_3$ species which serve as building blocks for the crystalline phase. Higher water concentrations also result in higher condensation rates, as evidenced by the rapid gelation of 1 : 3 samples. Higher building block concentrations and their relatively quick condensation in 1 : 2 compositions result in large regions having a similar structure to crystalline $LiNbO_3$. Since long distance diffusion within the matrix is not required, large-scale nucleation occurs earlier in films with a higher water ratio. Earlier nucleation allows for more time for grain growth in the films synthesized from the higher water concentration sols. Thus, the films with higher water contents have a larger grain size due to earlier crystallization.

Additional support for this suggestion is provided by DSC studies where the kinetic parameter $T_{crys}$, characterizing the onset of crystallization of $LiNbO_3$, shows a tendency to decrease as the added water of hydrolysis increases. Also, since the area under the DSC peak is proportional to the heat change involved, the latent heat of crystallization of the 1 : 2 gel is lower than that of the 1 : 1 gel. Although not conclusive, the accumulated observations indicate that increasing the amount of water of hydrolysis lowers the activation energy for crystallization of $LiNbO_3$, which we infer is due to an increased concentration of amorphous $LiNbO_3$ building blocks in the sol. This hypothesis could be verified with the help of NMR experiments.

Grain growth to dimensions similar to the 1 : 2 film occurred in the 1 : 1 film only at higher temperatures and/or longer soaking times. Unfortunately, this led to interfacial reactions at 600 °C. The presence of a Li deficient phase in the 1 : 1 film on glass is attributed to the elemental diffusion of Li into the substrate interface. Li diffusion is significant at 600 °C, as the activation energy for the diffusion of a small monovalent cation in silicate glasses is generally very low, ≈20 keV/g-atom.[23] However, diffusion of Li into the glass substrate does not play a significant role at 400 °C even with long soaking times (4 h). This is evident from the diffraction pattern of pure $LiNbO_3$ in Fig. 6(b).

(2) The second microstructural difference between the 1 : 1 and 1 : 2 amorphous and crystalline films of $LiNbO_3$ is the amount of porosity present. Porosity in the film is a function of sol structure.[24] As mentioned earlier, higher water concentrations lead to increased condensation rates. This increases size of precursor species in the sol. The progressive increase in porosity with precursor size is attributed to the rigid gel network which has a tendency to resist compaction during solvent evaporation. Figure 2, which illustrates the amor-

phous film structure for different water concentration sols, is in agreement with Brinker and co-workers.[25] They hypothesize that weak branching and low condensation rates during film formation allow the precursor to interpenetrate in response to the decreasing solvent concentration, promoting dense packing and low pore volume.

(3) The third microstructural distinction is associated with epitaxy of $LiNbO_3$ on sapphire. Low water concentrations (1 : 1) yielded epitaxial and single crystalline films, whereas higher water concentrations (1 : 2) yielded polycrystalline films with some preferred orientation. The single crystalline nature of 1 : 1 $LiNbO_3$ films but polycrystalline nature of 1 : 2 $LiNbO_3$ films on sapphire could be due to the competition between layer-by-layer solid phase epitaxy and random crystallization. The former phenomenon involves not only heteroepitaxial nucleation at the film-substrate interface but also subsequent homoepitaxial film growth on this initially nucleated layer. To ensure that the film retains its single crystal character, no two-dimensional nucleation of misoriented crystallites should occur.[26] This requires slow nucleation but a rapid lateral spreading rate. Braunstein *et al.*[27] were able to promote layer-by-layer solid phase epitaxy over random crystallization of sol-gel derived $SrTiO_3$ on (100) $SrTiO_3$ substrate by using high annealing temperatures, where surface diffusion was rapid. In our films, the lateral spreading rate is kinetically limited due to the low temperature of crystallization. The activation energy for heteroepitaxial nucleation on (0001) sapphire is lower than that for random nucleation of $LiNbO_3$ for 1 : 1 $LiNbO_3$ films, validated by the observation of single crystal epitaxy on (0001) sapphire instead of polycrystalline films. This difference in activation energy is narrowed for 1 : 2 $LiNbO_3$ films, where we postulate that higher concentration and aggregation of amorphous $LiNbO_3$ building blocks lowers the temperature for random nucleation. Heteroepitaxial nucleation should also occur concurrently with enhanced nucleation of random nuclei on the substrate surface in 1 : 2 films. The activation energy for crystallization is higher in 1 : 1 than 1 : 2, so the nucleation rate would be lower in 1 : 1 than 1 : 2. Therefore, we expect that epitaxy is easier for 1 : 1 films due to the lower random nucleation rate and the similar lateral spreading rate for 1 : 1 and 1 : 2 films.

The lateral growth of heteroepitaxial nuclei in 1 : 1 films followed by homoepitaxial growth in subsequent layers results in dense single crystalline $LiNbO_3$ films. However, since multiple heteroepitaxial nuclei are involved, they grow independently as islands. When they impinge, any mismatch is accommodated by the generation of defects such as stacking faults, twins, and dislocations, as seen in Figs. 8 and 9. In Fig. 10, moiré fringes reveal the periodicity of misfit between the $LiNbO_3$ and sapphire. The spacing of the moiré fringes corresponds to the predicted value for $(11\bar{2}0)$ $LiNbO_3$ on $(11\bar{2}0)$ sapphire. The presence of dislocations at the interface generated during film growth is also revealed in the moiré fringe pattern, visible as terminating fringes. An example of such a fringe is identified by the arrow in Fig. 10(a). These results also substantiate the interface nucleation for 1 : 1 films.

One final point that we wish to consider is the texturing of $LiNbO_3$ due to anisotropic surface energies. In our TEM studies on $LiNbO_3$ powders, we noted that at higher temperatures (600 °C) the growing particles further minimize their surface energy by acquiring faceted shapes. The face plane, plane of lowest surface energy, is the close-packed (0001) plane for $LiNbO_3$. In order to increase the (0001) surface area, the growth of the $LiNbO_3$ crystal in the [0001] direction is very slow and it grows rapidly in directions that are parallel to (0001). This is evident from the presence of hexagonal platelet particles at 600 °C. Matsunaga *et al.*[28] have also reported the tendency of $LiNbO_3$ films (deposited by ion plating) on glass substrates to orientate with the c-axis normal to the surface at 500 °C. As mentioned earlier, for the growth of epitaxial films a rapid lateral spreading rate is desired versus a high nucleation rate. It is possible that low temperature heteroepitaxial growth of $LiNbO_3$ is facilitated when its [0001] direction is perpendicular to the substrate. It is interesting to mention here that Nashimoto and Cima[9] had success in growing heteroepitaxial films on $(11\bar{2}0)$ sapphire at 400 °C only when they used unhydrolyzed sols while 1 : 1 $LiNbO_3$ films were oriented but polycrystalline.

## V. CONCLUSIONS

(1) Crystallization in double ethoxide derived $LiNbO_3$ was observed to begin in bulk gels at temperatures as low as 200 °C. The similarity in chemical short-range order between the double ethoxide and crystalline $LiNbO_3$ may facilitate this low temperature crystallization behavior. At higher temperatures (600 °C), hexagonal faceting of crystalline particles occurred with side facets being the first order prism planes and the large area faces the basal plane.

(2) Water of hydrolysis appeared to negligibly affect the chemical short-range order of the amorphous $LiNbO_3$ films, but DSC results showed a lower temperature of crystallization for higher water content sols. It is postulated that higher amounts of water lead to larger regions of $LiNbO_3$ building blocks in the sol, which lower the temperature of crystallization and activation energy of crystallization.

(3) Sols deposited on glass substrates having a low ethoxide-to-water ratio yielded dense and smooth polycrystalline films, whereas rough, porous films with a large grain size resulted from the use of sols with

increased water of hydrolysis. Earlier crystallization allowed for more grain growth.

(4) Low water content sols promoted epitaxial growth of dense $LiNbO_3$ on sapphire with nucleation at the substrate interface. The ease of random nucleation in high water content sols produced polycrystalline films with some oriented growth.

## ACKNOWLEDGMENTS

This work was supported through a grant from the Air Force Office of Scientific Research under Contract No. 49620-89-C-0050. The NSF Center for Interfacial Engineering at the University of Minnesota is acknowledged for the use of the CM30 TEM and Nanoscope II AFM.

## REFERENCES

1. R. S. Weis and T. K. Gaylord, Appl. Phys. A **37**, 191 (1985).
2. K. Nassau, H. Levinstein, and G. Loiacono, J. Phys. Chem. Solids **27**, 989 (1966).
3. K. Nassau and H. Levinstein, Appl. Phys. Lett. **7**, 69 (1965).
4. M. M. Abouelleil and F. J. Leonberger, J. Am. Ceram. Soc. **72**, 311 (1989).
5. G. Griffel, S. Ruschin, A. Hardy, M. Itzkovitz, and N. Croitoru, Thin Solid Films **126**, 185 (1985).
6. A. Okada, Ferroelectrics **14**, 739 (1976).
7. S. Hirano and K. Kato, J. Non-Cryst. Solids **100**, 538 (1988).
8. D. P. Partlow and J. Greggi, J. Mater. Res. **2**, 595 (1987).
9. K. Nashimoto and M. J. Cima, Mater. Lett. **10**, 348 (1991).
10. C-C. Hsueh and M. L. Mecartney, J. Mater. Res. **6**, 2208 (1991).
11. J. L. Keddie and E. P. Giannelis, J. Am. Ceram. Soc. **74**, 2669 (1991).
12. C. D. E. Lakeman and D. A. Payne, J. Am. Ceram. Soc. **75**, 3091 (1992).
13. V. Joshi, G. K. Goo, and M. L. Mecartney, in *Better Ceramics Through Chemistry V,* edited by M. J. Hampden-Smith, W. G. Klemperer, and C. J. Brinker (Mater. Res. Soc. Symp. Proc. **271**, Pittsburgh, PA, 1992), p. 377.
14. S. Hirano and K. Kato, Advanced Ceram. Mater. **3**, 503 (1988).
15. J. K. Bailey, J. R. Bellare, and M. L. Mecartney, in *Specimen Preparation for Transmission Electron Microscopy of Materials,* edited by J. C. Bravman, R. M. Anderson, and M. L. McDonald (Mater. Res. Soc. Symp. Proc. **115**, Pittsburgh, PA, 1988), p. 69.
16. S. M. Hues, R. J. Colton, E. Meyer, and H. J. Güntherodt, Mater. Res. Bull. **XVIII** (1), 41 (1993).
17. B. E. Warren, J. Am. Ceram. Soc. **17**, 249 (1934).
18. D. J. Eichorst and D. A. Payne, in *Better Ceramics Through Chemistry IV,* edited by B. J. J. Zelinski, C. J. Brinker, D. E. Clark, and D. R. Ulrich (Mater. Res. Soc. Symp. Proc. **180**, Pittsburgh, PA, 1990), p. 669.
19. D. J. Eichorst, K. E. Howard, and D. A. Payne (unpublished research).
20. A. Rauber, in *Current Topics in Materials Science,* edited by E. Kaldis (North-Holland, Amsterdam, 1978), p. 481.
21. A. M. Prokhorov and Y. S. Kuz'minov, *Physics and Chemistry of Crystalline Lithium Niobate* (Adam Hilger, Bristol and New York, 1990), p. 18.
22. D. J. Eichorst, D. A. Payne, S. R. Wilson, and K. E. Howard, Inorg. Chem. **29**, 1459 (1990).
23. W. D. Kingery, H. K. Bowen, and D. R. Uhlmann, *Introduction to Ceramics,* 2nd ed. (John Wiley & Sons, New York, 1976), pp. 257, 263.
24. C. J. Brinker and G. W. Scherer, *Sol-Gel Science* (Academic Press, New York, 1990), pp. 799, 814.
25. C. J. Brinker, A. J. Hurd, and K. J. Ward, in *Ultrastructure Processing of Advanced Ceramics,* edited by J. D. Mackenzie and D. R. Ulrich (John Wiley & Sons, New York, 1988), p. 223.
26. W. A. Tiller, *The Science of Crystallization–Microscopic Interfacial Phenomena* (Cambridge University Press, New York, 1991), pp. 171, 175.
27. G. Braunstein, G. R. Raz-Pujalt, M. G. Mason, T. Blanton, C. L. Barnes, and D. Margevich, J. Appl. Phys. **73**, 961 (1993).
28. H. Matsunaga, H. Ohno, Y. Okamoto, and Y. Nakajima, J. Cryst. Growth **99**, 630 (1990).